Cancer Research

CCR5 Receptor Antagonists Block Metastasis to Bone of v-Src Oncogene–Transformed Metastatic Prostate Cancer Cell Lines

Daniela Sicoli[1,2,3], Xuanmao Jiao[1,2], Xiaoming Ju[1,2], Marco Velasco-Velazquez[1,2,4], Adam Ertel[1,2], Sankar Addya[1,2], Zhiping Li[1,2], Sebastiano Andò[3], Alessandro Fatatis[2,5], Bishnuhari Paudyal[6], Massimo Cristofanilli[1,2], Mathew L. Thakur[2,6], Michael P. Lisanti[2,7], and Richard G. Pestell[1,2]

Abstract

Src family kinases (SFK) integrate signal transduction for multiple receptors, regulating cellular proliferation, invasion, and metastasis in human cancer. Although Src is rarely mutated in human prostate cancer, SFK activity is increased in the majority of human prostate cancers. To determine the molecular mechanisms governing prostate cancer bone metastasis, FVB murine prostate epithelium was transduced with oncogenic v-Src. The prostate cancer cell lines metastasized in FVB mice to brain and bone. Gene expression profiling of the tumors identified activation of a CCR5 signaling module when the prostate epithelial cell lines were grown *in vivo* versus tissue cultures. The whole body, bone, and brain metastatic prostate cancer burden was reduced by oral CCR5 antagonist. Clinical trials of CCR5 inhibitors may warrant consideration in patients with CCR5 activation in their tumors. *Cancer Res; 74(23); 7103–14. ©2014 AACR.*

Introduction

Prostate cancer remains the most common nondermatologic cancer in the United States and the second leading cause of cancer-related death among men with approximately 190,000 new cases diagnosed and approximately 27,000 deaths annually (1). The molecular mechanisms contributing to prostate cancer recurrence and therapy resistance are poorly understood. Increased expression of individual Src family kinases (SFK) has been observed during prostate cancer progression (2, 3). The SFK members Src and Lyn are highly expressed in the majority of human prostate cancers and Src kinase can promote prostate cancer initiation and progression (4). Androgen ablation therapy results in a 60% to 80% initial response rate (5). The majority of patients undergoing androgen antagonist therapy, however, subsequently relapse. Src has been strongly implicated in promoting androgen-independent growth and enhances androgen-induced proliferation of prostate cancer cells (6–8). Early diagnosis may provide an opportunity for curative surgery; however, approximately 30% of men who receive radical prostatectomy relapse, attributed to micrometastatic disease.

Prostate cancer is unique among solid tumors in its proclivity to metastasize primarily to bone. Once patients develop prostate cancer bone metastasis, the number of lesions increases dramatically, resulting in extensive pain and disability. Bone metastasis are common in many different cancer types including prostate, breast, lung, and colon, with some 350,000 people dying with metastasis to their bones each year in the United States (9, 10). The bone metastasis of prostate cancer is predominantly osteoblastic, although they often begin as osteolytic lesions (11).

A number of studies have sought to identify molecular drivers of metastasis based on groundbreaking work by Filder (12) and Kim and colleagues (13). Metastatic prostate cancer has a unique predilection for bone with significant clinical consequence. The immune system contributes to the onset, progression, and metastases of prostate cancer. At this time, there is a relative paucity of animal models that undergo reliable metastasis to bone (14, 15). Thus, although transgenic mice maintain a normal immune response, none of the current transgenic models undergo reliable bone metastasis.

Analysis of the molecular mechanisms governing bony metastasis of prostate cancer requires the development of prostate cancer cell lines that spread reproducibly to bone in

[1]Department of Cancer Biology, Thomas Jefferson University, Philadelphia, Pennsylvania. [2]Sidney Kimmel Cancer Center, Thomas Jefferson University, Philadelphia, Pennsylvania. [3]Faculty of Pharmacy, Nutrition, and Health Science, University of Calabria, Arcavacata di Rende, Italy. [4]Departamento de Farmacología, Facultad de Medicina, Universidad Nacional Autónoma de México, México City, México. [5]Department of Pharmacology and Physiology, Drexel University, Philadelphia, Pennsylvania. [6]Department of Radiology, Thomas Jefferson University, Philadelphia, Pennsylvania. [7]Stem Cell Biology and Regenerative Medicine, Thomas Jefferson University, Philadelphia, Pennsylvania.

Note: Supplementary data for this article are available at Cancer Research Online (http://cancerres.aacrjournals.org/).

D. Sicoli and X. Jiao contributed equally to this article.

Current address for M.P. Lisanti: The Manchester Centre for Cellular Metabolism and The Breakthrough Breast Cancer Research Unit, The University of Manchester, Manchester, United Kingdom.

Corresponding Author: Richard G. Pestell, Department of Cancer Biology, Sidney Kimmel Cancer Center, Thomas Jefferson University, Room 1050 BLSB, 233 South 10th Street, Philadelphia, PA 19107. Phone: 215-503-5692; Fax: 215-503-9334; E-mail: director@kimmelcancercenter.org

doi: 10.1158/0008-5472.CAN-14-0612

immunocompetent mice. The lack of robust animal models of bone metastasis has hampered the development of new therapeutics. To address this question, we developed isogenic oncogene-transduced murine prostate epithelial cancer cell lines (16). These cell lines reliably formed osteolytic bone lesions in immunocompetent mice. Gene expression analysis comparing the cell lines in tissue culture with gene expression of the tumors in immune competent mice evidenced the activation of CCR5 signaling axis. Inhibition of the CCR5 signaling module by drug treatment blocked bone and brain metastasis.

Materials and Methods

Cell culture, transfection, transduction, and expression vectors

The prostate epithelial cells (PEC) were transformed with the v-Src oncogene, generated in this laboratory (16), were transduced with a lentiviral vector containing the luc2 and Tomato Red genes to generate stable bioluminescent cancer cell lines. [The Luc2-tomato red expression vector (Luc-Tom) has been described previously (17)]. The isogenic v-Src-PEC lines were maintained in DMEM supplemented with 10% FBS and 1% penicillin–streptomycin and cultured in 5% CO_2 at 37°C. MG132 was purchased from Calbiochem and was used at the concentration of 10 μmol/L for 12 hours.

Wound healing assay

Cells were grown to confluence on 12-well plates in DMEM containing 10% FBS. The monolayers were wounded with a P10 micropipette tip. The cells were washed with PBS immediately after scoring and serum-free DMEM was added (18). Wound healing was monitored using an Axiovert 200 Zeiss microscope system for 20 hours. Video images were collected with a CCD camera (model 2400) at 20-minute intervals, digitized, and stored as images using Metamorph software. Images were converted to QuickTime movies and the position of nuclei was tracked to quantify cell motility. Cellular velocity was calculated in micrometers (μm) using Metamorph software. The movie of cell migration was taken at 20 minutes per frame for 20 hours using an Axiovert 200 Zeiss microscope system. Images were analyzed using MetaMorph software.

Tumor formation assay

Male FVB mice, 12-week-old, were anesthetized by exposure to 3% isoflurane. Anesthetized mice received 1×10^6 cells suspended in 50 μL of Dulbecco PBS lacking calcium and magnesium (DPBS) and 50 μL of BD Matrigel Basement Membrane Matrix (BD Biosciences) by subcutaneous injection at one dorsal flank. The injection was performed using 27.5-gauge needle. Tumor progression was followed by measurement of bioluminescence once a week until tumor excision, using the IVIS LUMINA XR system (Caliper Life Sciences) as described previously (19). Briefly, for *in vivo* imaging, mice received the substrate of luciferase, D-Luciferin (Gold Biotechnology), at 15 mg/mL in PBS by intraperitoneal injection of 10 μL of luciferin stock solution per gram of body weight (manufacturer's recommendation) and were anesthetized by exposure to 3% isoflurane. At 10 to 15 minutes after D-luciferin injection, animals were placed inside the camera box of the IVIS Lumina XR and received continuous exposure to 2.5% isoflurane. Imaging time ranged from 5 minutes (for earlier time points) to 5 seconds (for later time points), depending on the bioluminescence of neoplastic lesion. Regions of interest (ROI) from displayed images were drawn around the tumor sites or the metastatic lesion and quantified using the Living Image 3.0 software (Caliper Life Sciences). Tumor samples were harvested after 3 weeks. All experiments involving mice were carried out under the approval of Institutional Animal Care and Use Committee (IACUC) of the Thomas Jefferson University (Philadelphia, PA).

Experimental metastasis assay

Eight-week-old male FVB mice were anesthetized by exposure to 3% isoflurane. A total of 2×10^5 cancer cells suspended in 100 μL of DPBS were injected into the left ventricle of the heart of the mouse. Injections were performed using a 30.5-gauge needle and a 1-mL syringe. To confirm the presence of cells in the systemic circulation, animals were imaged using IVIS LUMINA XR system as described above. A successful intracardiac injection was indicated by systemic bioluminescence distributed through the animal body. Mice not properly injected were removed from the study. Results were analyzed using Living Image 3.0 software.

Radiographic analysis of bone metastasis and CT

Development of bone metastasis was monitored by X-ray radiography using the IVIS Lumina XR. Mice were anesthetized, arranged in a prone position, and exposed to an X-ray for 5 minutes.

Administration of maraviroc (antagonist of CCR5)

Male FVB mice received an oral dose of maraviroc (Selleck Chemicals LLC) of 8 mg/kg every 12 hours from 5 days before inoculation of cancer cells until euthanasia. The drug was dissolved in acidified water containing 5% DMSO. Control mice were maintained on an identical dosing schedule and received the same volume of vehicle.

Invasion assay

The three-dimensional invasion assay was performed as previously reported (20). Briefly, 100 μL of 1.67 mg/mL Rat Tail Collagen Type I (BD Biosciences) was pipetted into the top chamber of a 24-well 8-μm pore Transwell (Corning). The Transwell was incubated at 37°C overnight to allow the collagen to solidify. Thirty-thousand cells were then seeded on the bottom of the Transwell membrane and allowed to attach. Serum-free growth medium was placed into the bottom chamber, whereas 15 ng/mL CCL5 (R&D Systems), or 10% FBS was used as a chemoattractant in the medium of the top chamber. The cells were then chemoattracted across the filter through the collagen above for 3 days. Cells were fixed in 4% formaldehyde, permeabilized with 0.2% Triton-X in PBS, and then stained with 40 μg/mL propidium iodide for 2 hours. Fluorescence was analyzed by confocal z-sections (one section every 20 μm) at ×10 magnification from the bottom of the filter

using a Zeiss LSM 510 Meta inverted confocal microscope at the Kimmel Cancer Center Bioimaging Facility.

Histologic analysis

Tumor samples and soft tissues were fixed in 4% paraformaldehyde (PFA, Fisher Scientific) and processed for paraffin embedding, sectioning, H&E, and immunohistochemistry (IHC). Bones were fixed in 4% PFA at 4°C for 72 hours, decalcified in 0.5 mol/L EDTA (pH 8.0) for 7 days at 4°C, and embedded in paraffin (21). Antibodies for IHC were CK5 (PRB-160P, Covance), CK8 (MMS-162P, Covance), KLK3 (Ab44392, Abcam), and CCR5 (A00979, GenScript) for staining of tumor sections. CK5 staining was performed after deparaffinization and rehydration without the antigen retrieval treatment on bone and brain samples to confirm the presence of basal prostate epithelial cells. CK8 staining needed pretreatment of slides with a citrate buffer retrieval solution (Biogenex) and was performed to show the presence of luminal prostate epithelial cells in bone and brain samples. Tartrate-resistant acid phosphatase (TRAP) staining was performed after deparaffinization and rehydration as directed by the manufacturer (Sigma-Aldrich) to identify active osteoclasts at the surface between metastatic lesion and compact bone (22, 23). The tetrachrome method was performed on bones to identify woven bone in the osteoblastic lesions areas (22, 24).

Cell labeling and FACS analysis

Before labeling, the cells were blocked with normal mouse IgG in 1/100 dilution for 1 hour and then incubated with APC-labeled mouse anti-human/mouse CCR5 (1/10; FAB1208A, R&D Systems) for another hour. APC-labeled normal mouse IgG was used as negative control. All experiments were carried out at 4°C. Cell sorting was performed on FACSCalibur flow cytometer (BD Biosciences). The data were analyzed with FlowJo software (Tree Star, Inc.).

Microarray analysis methods

Preprocessing and differential expression analysis. Microarray data were preprocessed using background correction, and quantile normalization and summarization were performed on the Mouse Gene 1.0 ST gene expression microarrays using the Robust Multichip Analysis workflow in Affymetrix Expression Console version 1.1 (Affymetrix, Inc.). Differentially expressed genes were identified for the v-Src-PEC tumor, by performing pairwise comparisons against the normal mouse prostate or v-Src-PEC cell culture. These comparisons were performed using significance analysis of microarrays (SAM) with a false discovery rate cutoff of 1% and 2-fold change cutoff.

PET imaging

Animal imaging was performed according to the IACUC. Flourine-18, sodium fluoride (F-18-NaF) in isotonic solution was obtained from IBA Molecular. A total of 210 ± 9.54 μCi of F-18-NaF in 150 μL was injected through the lateral tail vein of unanesthetized mice. One hour later, animals were anesthetized with 1.5% isoflurane in 98.5% O_2 and imaged with the Inveon microPET scanner (Siemens Hoffman estate), a high spatial resolution (1 mm in full-width at half maximum) and sensitivity (>10%) position emission scanning (PET) scanner. On average, 1.5 million counts were obtained in 10 minutes of imaging. An ordered subset expectation maximization 3-dimensional algorithm with 5 iterations and 8 subsets was used for demonstration.

X-ray imaging

The images were acquired using CareStream Molecular Imaging FX-Pro scanner. Image capture setting was set to X-ray imaging performed at an energy of 35 KVP and an X-ray current of 150 μA with a total acquisition time of 60 seconds. The radio phosphor screen was positioned in the imaging field. The exposure type was set to Standard with X/Y binning set to none to increase image resolution. Emission and Excitation filters were both set to zero. FOV was set to 120.0 mm with an f-stop of 2.80 and a focal plane of 7.6 mm. During imaging, each mouse was anesthetized by inhalation of 1.5% isofluorane and 98.5% O_2. The bright field images were captured and digitized.

Optical density analysis

CareStream molecular Imaging FX-Pro software allows optical density (OD) to be measured by using the amount of light that passes through an object to determine the amount of matter within an ROI. Optical density was performed on both tibias of each of the treated (3) and untreated (3) mice with 6 ROIs drawn on each tibia. The total tibia mean OD of each mouse was then tabulated for each mouse and the OD was compared between the treated and untreated mice.

Statistical analysis

Comparisons between groups were analyzed by two-sided *t* test. A difference of $P < 0.05$ was considered to be statistically significant. All analyses were done with SPSS 11.5 software. Data are expressed as mean ± SEM.

Results

V-Src prostate cancer tumor growth in immunocompetent mice

The v-Src prostate cancer cell lines derived by transduction of murine prostate epithelial cells with retroviruses encoding oncogenic v-Src and Luc2-Tomato were assessed for invasive and growth properties. The v-Src-PECs were assessed for migration in wound-healing assays. Comparison was made with the parental nontransformed PEC. The velocity of the cell moving to wound strip was measured quantitatively for 12 hours. The velocity of migration was increased 73.3% from 0.57 ± 0.06 μm/minute to 0.99 ± 0.12 μm/minute (Fig. 1A and B). The v-Src PEC cells also conveyed the ability to invade Matrigel, whereas the parental PECs were unable to invade (Fig. 1C).

The v-Src-PEC grew as subcutaneous tumors in immunocompetent FVB mice. The relative abundance of several proteins was determined by immunohistochemistry with comparison made to sections of normal prostate from FVB mice. Androgen receptor (AR) abundance was reduced (Fig. 2B). Immunohistochemical analysis of the tumors identified the presence of cytokeratins CK5 and CK8 (Fig. 2C and D). CK5 is a

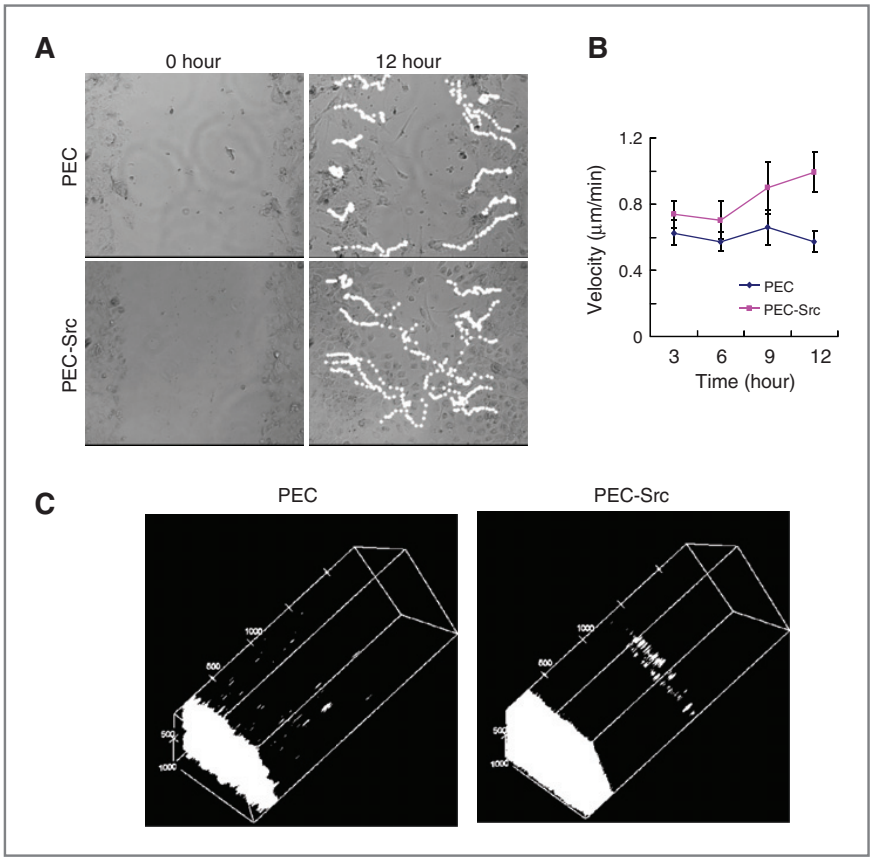

Figure 1. v-Src enhances prostate cancer cell lines invasion. A, wound-healing assay showing increased cellular migration of v-Src-PEC into the wound compared with parental PEC. B, quantitation of cell movements (velocity) by tracking single-cell movement for $N = 12$. C, three dimensional Matrigel invasion showing v-Src-PEC has increased invasive ability compared with normal PEC.

marker of basal cell type origin, which is more common in metastatic prostate cancer upon androgen deprivation (25), was increased, whereas CK8 was reduced (Supplementary Fig. S1). The tumors expressed the androgen-responsive KLK3 (glandular kallikrein-related peptidase 3), consistent with expression of AR by this line in tissue culture (16). Quantitation of AR mRNA levels by quantitative real-time PCR (qRT-PCR) demonstrated a relative reduction in AR mRNA levels compared with primary prostate epithelial cells (Fig. 2F). Western blot analysis of the v-Src lines in tissue culture demonstrated a reduction in AR and CK8 but an increase in CK5 abundance compared with the parental PEC when normalized to the loading control vinculin (Supplementary Fig. S2A). Immunostaining of individual v-Src PEC demonstrated the cells consisted of a heterogeneous mixture of both CK5- and CK8-stained cells (Supplementary Fig. S2B).

The v-Src prostate cancer lines metastases to bone and brain

Upon introduction of the v-Src-PEC line into the arterial circulation via intracardiac injection, tumors developed in multiple organs within two weeks of injection (Fig. 3). Photonic emission evidenced metastasis to the brain, bones, kidney and liver (Fig. 3C–E). The relative frequency of metastasis amongst the mice was determined as 100%. The relative tumor burden for each organ was consistent for each of the mice injected with the v-Src-PEC cell lines (Fig. 3E). One hundred percent of the v-Src-PEC–injected mice developed bony metastasis. The bony photon flux was dramatically enhanced in the v-Src-PEC tumors, with total photon flux (5×10^7) (Fig. 3D).

v-Src–induced prostate tumor metastasis maintain the histologic features of the primary prostate tumors

We characterized the bone metastasis of the v-Src-PEC lines. In view of the importance of generating a model of prostate cancer metastasis that reflects human disease, we conducted complementary approaches to analysis of the bone lesions. X-ray of the bones at day 14 demonstrated the presence of radiolucent lesions in the tibia (Fig. 4A); femur, spine, and skull. The bony metastasis of the mice were osteolytic in nature by X-ray (Fig. 4A). The lesions were found primarily at the epiphyseal junction as osteolytic lesions at two weeks (Fig. 4E). The X-ray rendered images were next characterized by surface rendering (Fig. 4B) and by CT scan (Fig. 4B). Each of these imaging techniques confirmed the presence of bone lesions.

TRAP is a glycosylated monomeric metallo-enzyme expressed in osteoclasts. The prostate cancer bone lesions were surrounded by TRAP positive cells, suggesting prostate

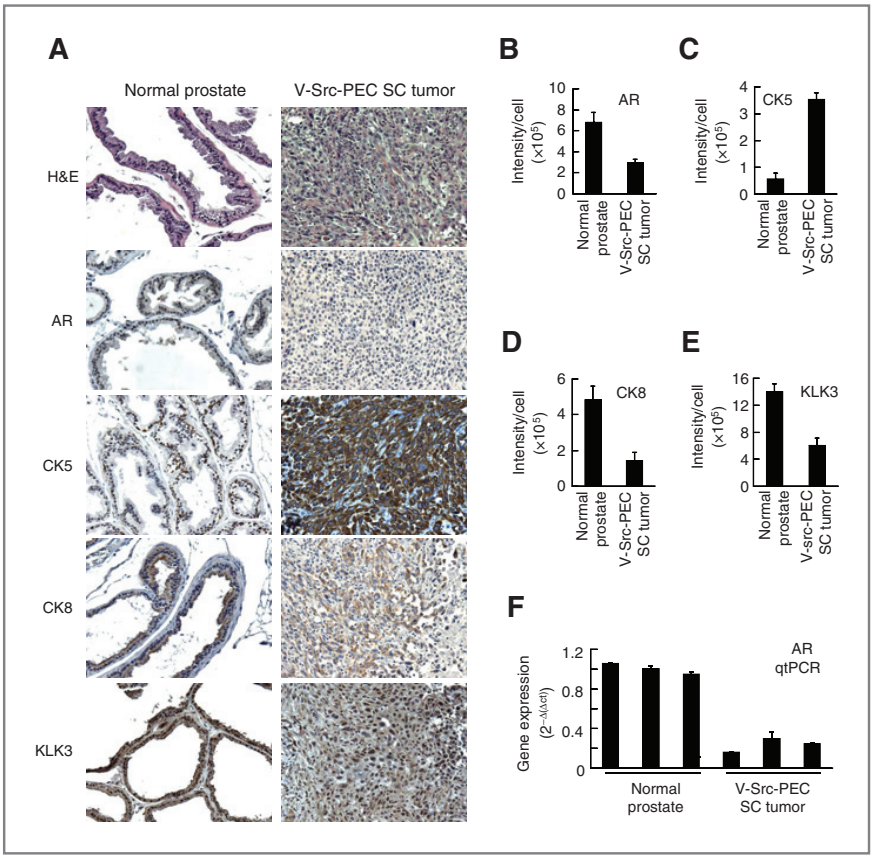

Figure 2. A, H&E staining and immunohistochemical staining of v-Src-PEC tumor in FVB mice for AR, the basal prostate epithelial cell marker CK5, the luminal prostate epithelial cell marker CK8, and prostate cell marker KLK3. Quantitative analysis of immunohistochemical staining signal intensity is shown as AR (B), CK5 (C), CK8 (D), and KLK3 (E). CK5 was increased in v-Src-PEC tumor compared with in normal prostate, whereas CK8, AR, and KLK3 were decreased. The decrease of AR expression was confirmed by qRT-PCR (F).

cancer metastasis induced an osteoclastic reaction, typically found with osteolytic lesions, as observed histologically (Fig. 4C). As TRAP can also be expressed in activated macrophages further histological confirmation was conducted of the bony metastasis. Histological analysis of the osteolytic bone lesions of the prostate tumors evidenced adenocarcinoma resembling the primary tumor. Hematoxylin and eosin (H & E) staining identified the histological features of the metastatic tumor as similar to the primary adenocarcinoma (Fig. 4D), and the adenocarcinoma cells stained positive for the prostate basal epithelial cell marker CK5 (Fig. 4E), CK8, and KLK3 (Fig. 4F, G, and Supplementary Fig. S3).

CCR5 signaling is enhanced in v-Src–induced prostate tumors grown in immunocompetent mice *in vivo*

In order to determine the genetic pathways induced by v-Src transformation of prostate epithelial cells, comparison was made of microarray gene expression from multiplicate normal mouse prostate tissues and multiplicate independent v-Src-PEC tumors generated by subcutaneous injection (Fig. 5A). GO term analysis was conducted and the results displayed in two dimensions of fold enrichment and the number of genes for each GO term identified. The GO terms of cytokine–cytokine receptor interaction and chemokine signaling were significantly enriched (Supplementary Fig. S4A). Within these GO terms, components of the CCR5 signaling pathway were significantly upregulated by v-Src (Fig. 5B). In order to determine which pathways were regulated by tumor growth *in vivo*, comparison was made between the v-Src–transformed lines grown in tissue culture, with the v-Src-transformed PEC growth in immune competent FVB mice. GO term analysis of multiplicate independent cell lines demonstrated again enrichment of the cytokine–cytokine receptor interaction GO term and the chemokine signaling pathways (Supplementary Fig. S4B). Microarray comparison demonstrated increased expression of specific cytokine receptors and their ligands including CCR7, CCR5, CCRl, CCL8, CCL7, CCL2 and CCL1 (Fig. 5C). The relative changes in gene expression are shown colorimetrically (Fig. 5C, Supplementary Fig. S5B) or quantitatively (Fig. 5D). CCR5 serves as a receptor for several ligands including CCL5, CCL8 and CCL7 (Fig. 5E). The increased expression of CCR5 (11.3-fold), CCL7 (5.2-fold) and CCL8 (8.6-fold) may be expected to enhance signaling by this receptor. Interrogation of Oncomine data for human prostate cancer demonstrated a moderate but significant increase in CCR5 abundance in patient lymph node and bone metastasis (Fig. 5F). Increased CCR5 expression was also observed in human prostate cancer compared with benign disease and in metastatic compared

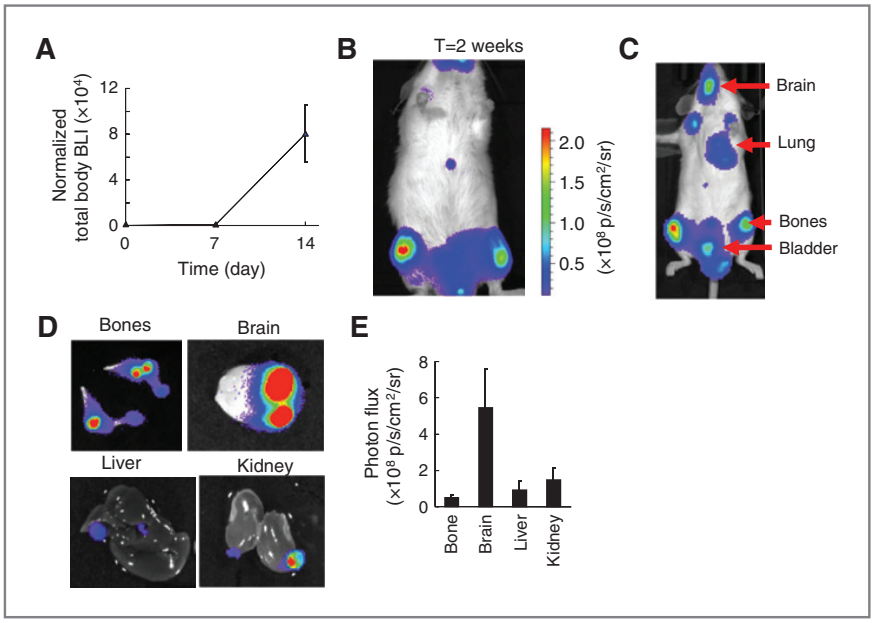

Figure 3. v-Src PEC metastasize to bone and brain. A, total body bioluminescence (BLI) at 2 weeks after intracardiac injection of v-Src-PEC. The v-Src-PECs transduced with the Luc2-Tom expression vector were injected into the left cardiac ventricle. $N = 5$ of FVB mice and the *in vivo* bioluminescent signal was quantified weekly. B and C, representative *in vivo* images of mice with brain, lung, bone, and bladder metastasis are shown. D, representative images of BLI from metastasis to each organ are indicated in the figure. E, mean total proton flux as a measure of metastatic tumor burden for each of the isogenic lines. Data are mean ± SEM, $n = 5$.

with primary disease in other public databases (Supplementary Fig. S7A–C). A gene signature that included CCR5, generated from the chemokine signaling pathway to include genes upregulated in both *in vivo* tumor versus *in vitro* cell culture and in v-Src-PEC tumor versus in normal prostate, was highly correlated with recurrence-free survival probability of patients in both the Glinsky and Tailor data sets (Supplementary Fig. S7D–G). FACS analysis of the v-Src-PEC demonstrated that 25.4% of the cells expressed CCR5 protein on the cell surface (Fig. 5G). In view of the CCR5 receptor activation in the v-Src-PEC and recent studies demonstrating CCR5 promotes invasion and metastasis of basal breast cancer cell lines in immune-deficient mice (26), we examined the role of CCR5 in v-Src-PEC cellular invasion. Matrigel invasion by the v-Src-PEC was abolished by the CCR5 inhibitor maraviroc (Fig. 5H). The v-Src-PEC line was injected into FVB mice and animals were treated with either oral maraviroc or control for 2 weeks. Representative examples of the mice are shown in Fig. 5I. The total body metastasis tumor burden was reduced by >60% upon Maraviroc treatment (Fig. 5J). Immunohistochemical staining identified the presence of CCR5 within the bone metastasis that was identified by histology as adenocarcinoma (Fig. 5K).

To determine the mechanism by which v-Src induces CCR5 abundance, qRT-PCR was conducted for CCR5 mRNA levels comparing the v-Src-PEC tumors with the normal prostate tissues (Supplementary Data 6). The CCR5 mRNA levels were increased 4- to 5-fold in v-Src-PEC tumors. To determine whether v-Src contributes to CCR5 protein stability, cells were treated with proteasome inhibitors for 12 hours and the relative amount of $CCR5^+$ cells assessed by FACS (Supplementary Fig. S8). The proteasome inhibitor MG132 enhanced the proportion of CCR5 positive cells approximately 6-fold (Supplementary Fig. S8). The Src inhibitor dasatinib reduced the proportion of CCR5 positive cells by 50%, consistent with the role of Src kinase in the enhancement of CCR5 abundance in the presence of proteasome inhibitor.

The CCR5 inhibitor maraviroc reduces v-Src prostate tumor bone metastasis in immunocompetent mice

In view of the findings that the metastatic bone tumors expressed CCR5, we examined the effect of CCR5 inhibition on the bone metastasis burden. Radiologic imaging evidenced tibial periphyseal metastasis of control animals (Fig. 6A). The animals treated with maraviroc for the same time period demonstrated a reduction in the tibial periphyseal osteolucent lesions. For quantification of total body bone burden, the bone photon flux was quantitated after 2 weeks for $N = 10$ animals (Fig. 6B) and demonstrated an approximately 80% reduction in bone metastatic burden. Representative examples of the control (Fig. 6C–G) or maraviroc-treated animals (Fig. 6H–L) illustrate photonic emission of tumors (Fig. 6C and H), the PET (Fig. 6D, E, I, and J) and PET/CT scanning (Fig. 6F, G, K, and L).

The CCR5 inhibitor maraviroc reduces v-Src prostate brain metastasis in immunocompetent mice

We next determined the effect of CCR5 inhibition on the v-Src-PEC brain metastasis. Histologic analysis demonstrated the presence of prostate adenocarcinoma by H&E staining (Fig. 7A). The brain metastasis was immunopositive for CK5, CK8, and KLK3 (Fig. 7A–D). Oral maraviroc administration reduced the brain metastasis burden with a representative example shown in Fig. 7E. Quantitative analysis for $N = 10$ animals demonstrated a >60% reduction in tumor burden (Fig. 7F and G).

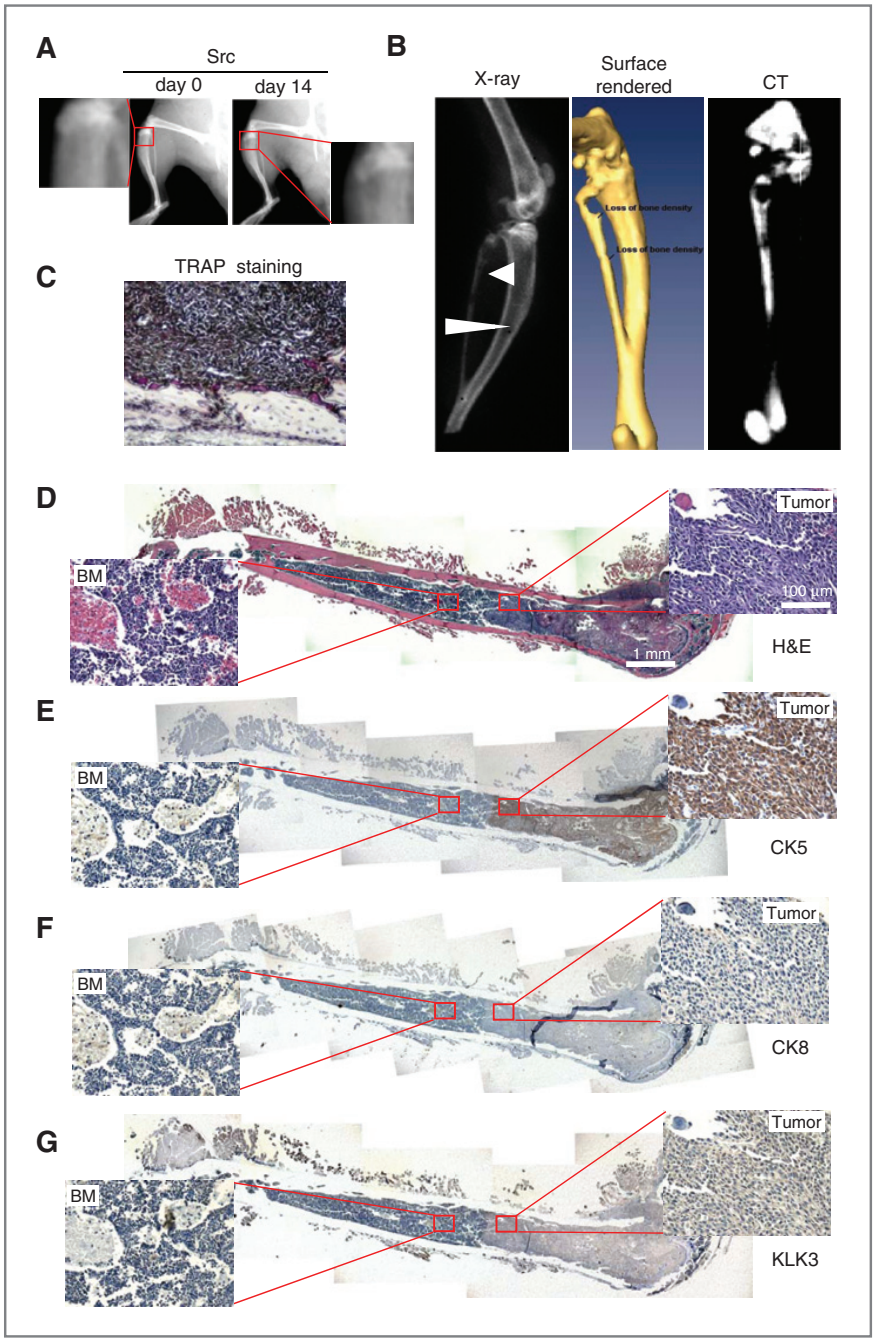

Figure 4. Prostate cancer bone metastases. v-Src-PEC lines transduced with Luc2-Tom were injected into FVB mice and histologic analysis was conducted of regions corresponding to the *in vivo* bioluminescent signal. A, X-ray of osteolytic lesion before (t0) and 14d (t14) after intracardiac injection of cells. Low density areas colocalized with the metastatic tumors (arrowhead), indicating osteolytic lesions. B, comparison of X-ray, surface rendering, and CT image of bone tumors. C, TRAP staining of region surrounding bone lesion. D, H&E staining of bone metastasis and immunohistochemical staining of metastatic tumors for CK5 (E), CK8 (F), and KLK3 (G).

Discussion

The current studies provide several lines of evidence that v-Src oncogene transformation of prostate epithelium induces metastatic prostate cancer cells associated with increased expression of CCR5 signaling activity. Comparison of non-transformed and v-Src-PEC demonstrated v-Src induces expression of both the receptor and ligands that contribute to activation of CCR5 signaling. Further enhancement of CCR5 signaling components was demonstrated in tumors grown in immunocompetent mice. IHC demonstrated the presence of CCR5 in the v-Src-PEC bone metastasis. Treatment with the CCR5 inhibitor maraviroc reduced tumor metastasis size.

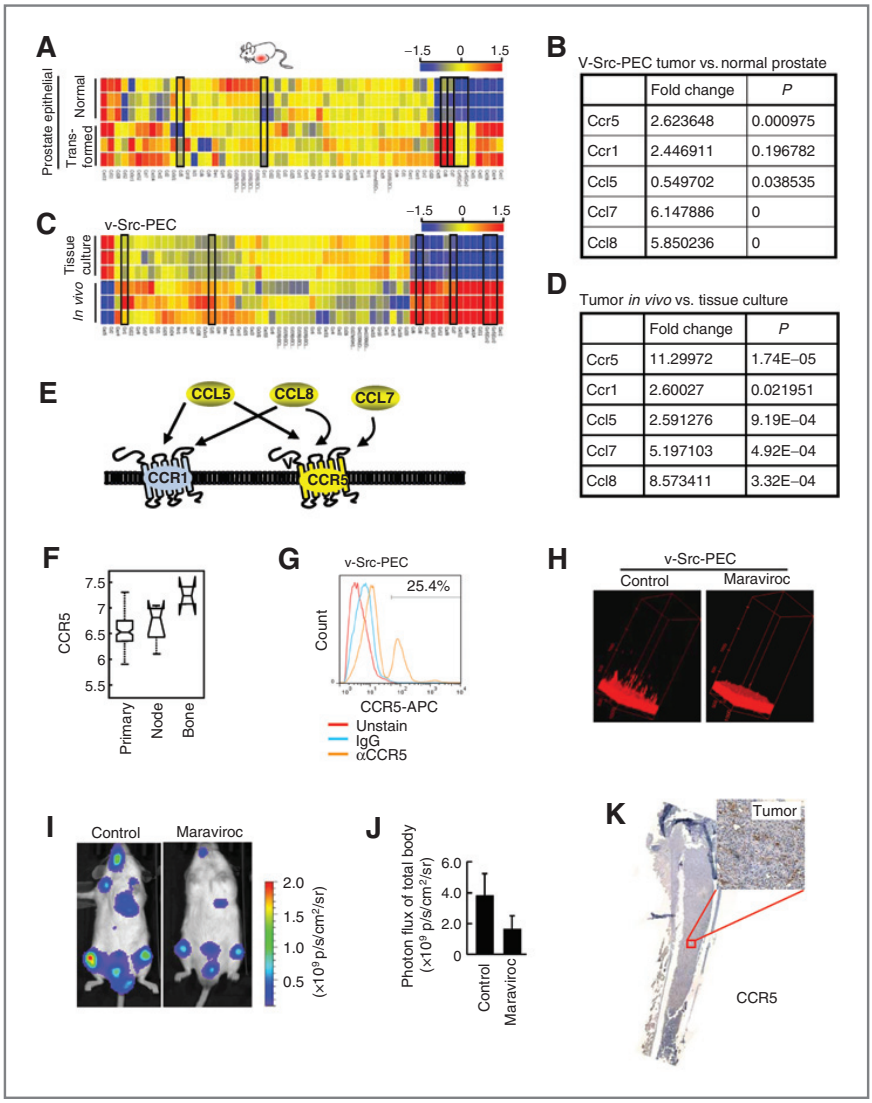

	Fold change	*P*
Ccr5	2.623648	0.000975
Ccr1	2.446911	0.196782
Ccl5	0.549702	0.038535
Ccl7	6.147886	0
Ccl8	5.850236	0

	Fold change	*P*
Ccr5	11.29972	1.74E−05
Ccr1	2.60027	0.021951
Ccl5	2.591276	9.19E−04
Ccl7	5.197103	4.92E−04
Ccl8	8.573411	3.32E−04

Figure 5. Induction of CCR5 signaling in v-Src-PEC tumors grown in immunocompetent mice *in vivo*. A, gene expression profile comparing normal FVB murine prostate epithelial cells with v-Src–transformed FVB murine prostate epithelial cells. B, relative abundance of ligands and receptors in CCR5 pathway. C, comparison of gene expression of v-Src PEC grown in tissue culture or in FVB mice. The relative expression levels are shown as a color gradient or as mean changes in gene expression for $N = 3$ separate v-Src PEC tumors (D). E, schematic representation of CCR5 signaling pathways. F, gene expression data from Oncomine for primary prostate cancer lymph node and bone metastasis. G, FACS analysis for CCR5 expression comparing PEC with v-Src-PEC, illustrating enrichment upon v-Src transformation (25%). H, Matrigel invasion arrays of v-Src-PEC conducted in the presence of control or CCR5 inhibitor maraviroc. I and J, representative photon images of FVB mice injected with v-Src-PEC treated with either control or maraviroc for 16 days (I), and mean data ±SEM for CCR5 in v-Src PEC bone metastasis (J). K, immunohistochemical staining for CCR5 in v-Src-PEC metastasis in bone (high resolution image is shown in Supplementary Data S1).

Together, these findings strongly suggest the CCR5 pathway is activated in v-Src-PEC *in vitro* and *in vivo*.

The current studies demonstrate the development of a murine model that recapitulates human prostate cancer in several important ways. First, the current studies deployed, v-Src-PEC, which activated SFK, as observed in the majority of patients with prostate cancer. Second, the tumor histology reflects human prostate adenocarcinoma. Third, the current metastatic prostate cancer model was developed in immunocompetent mice. The immune system contributes to the onset and progression of human prostate cancer metastasis and the v-Src-PEC metastasized in immunocompetent FVB mice. Fourth, the gene expression profile is enriched in a subset of patients with prostate cancer (16). Together, these findings suggest this model may be a useful complement to the currently available preclinical models of prostate cancer.

The understanding of the molecular mechanisms governing prostate cancer metastasis and the development of prostate cancer metastasis therapies has been limited by the lack of preclinical models that faithfully recapitulate human diseases (15). Transgenic mouse models of prostate cancer either fail to develop bone metastasis (27–29) or have such low penetrance of metastasis, therefore the impact of treatment cannot be effectively ascertained (28). Several laboratories have focused on metastatic sublines of tumor cells developed through *in vivo* selection or clonal expansion comparing expression profiles of highly and nonmetastatic counter parts from isogenic backgrounds. One recent report of the RM1 cell line developed from murine urogenital sinus tumors implanted onto the kidney capsule developed metastasis after intracardiac injection with high frequency in derivative RM1 (BM) (22). Additional studies have looked at metastasis-promoting and metastasis-

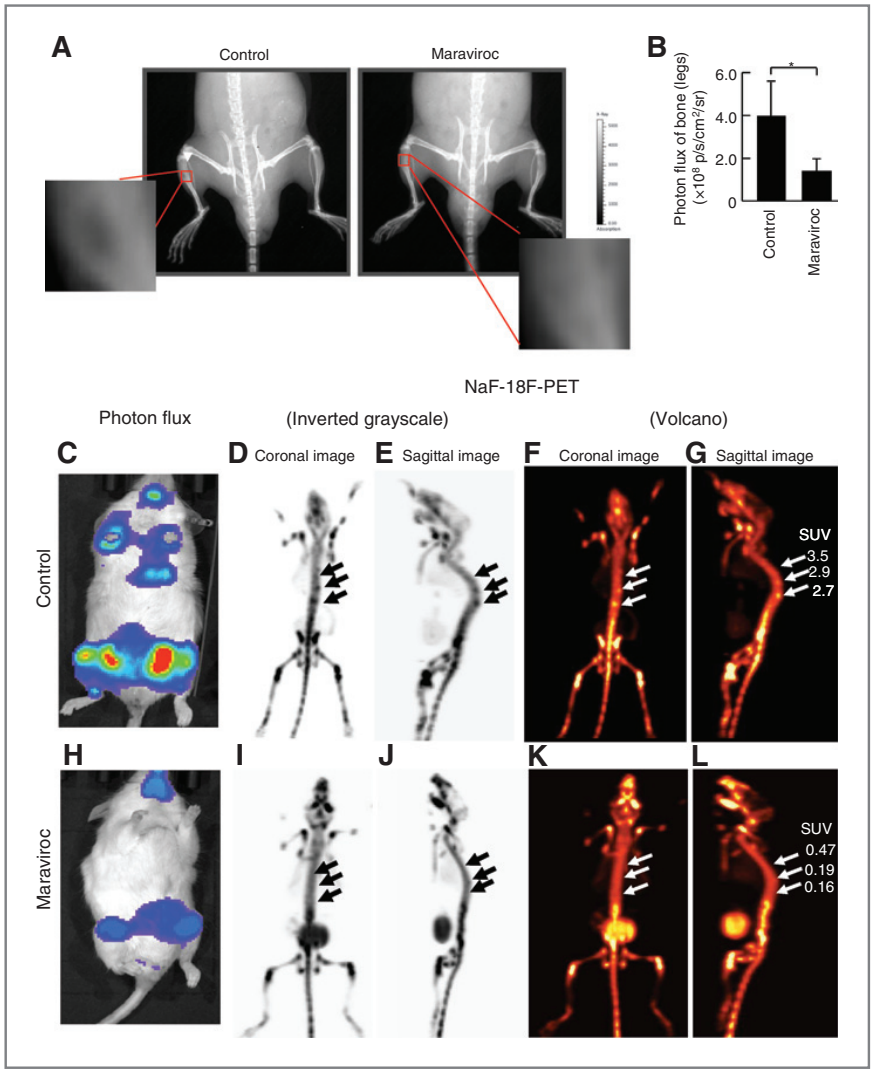

Figure 6. The CCR5 antagonist maraviroc reduces v-Src-PEC bone metastasis in immunocompetent mice. A and B, representative X-ray of FVB mice after injection with v-Src-PEC, treated with control or maraviroc comparing X-ray of proximal tibia (A), and photon flux of tumors in tibia shown as mean ±SEM for $N = 10$ separate mice (B). C and H, representative images of v-Src PEC photon flux. D and E versus I and J, PET images shown as inverse gray scale and F and G versus K and L shown as volcano images.

suppressing genes (30). Specific subsets of genes have been identified that mediate breast cancer metastasis to bone (31–36).

The current studies demonstrate that oncogenic Src induces CCR5 signaling in prostate epithelial cells. CCR5 has been shown to promote breast cancer metastasis via a homing mechanism (26). Src has been implicated in activation of the AKT survival pathway, and Src is required for CXCLR activation in metastatic breast cancer cells (13). These findings may have useful clinical implications. SFKs have been considered as potential drug targets in human prostate cancer. Src inhibitors reduce prostate cancer growth in mouse xenograft studies (37) and in regenerative prostate grafts (6). In prior studies using a model of c-Src and AR-transduced prostate epithelial cells with transplantation under the kidney capsule in immunodeficient (SCID) mice, dasatinib reduced tumor graft weight (6). Dasatinib, saracatinib, and basutinib are three SFK inhibitors that exhibit clinical efficacy. Toxicity, however, includes reduced renal tubular secretion of creatinine and centrosomal and mitotic spindle defects in normal cells and cardiac toxicity (38–40). Severe adverse clinical symptoms include renal failure, fatigue leniency, anorexia, vomiting, and diarrhea (41). Src activates distinct signaling modules. The ability to identify a tractable Src-dependent module that contributes to tumor metastasis, governing CCR5 signaling as shown herein, presents a rational alternative therapeutic approach.

The relevance of the current studies is supported first by interrogation of human prostate cancer samples demonstrating increased expression of CCR5 in bone metastasis compared with the primary tumor. Second, in recent studies, an algorithm was developed that distinguished good and poor prognosis of patients with prostate cancer (16). Components of the chemokine signaling pathway, including CCR5, were significantly enriched in the poor prognosis signature group

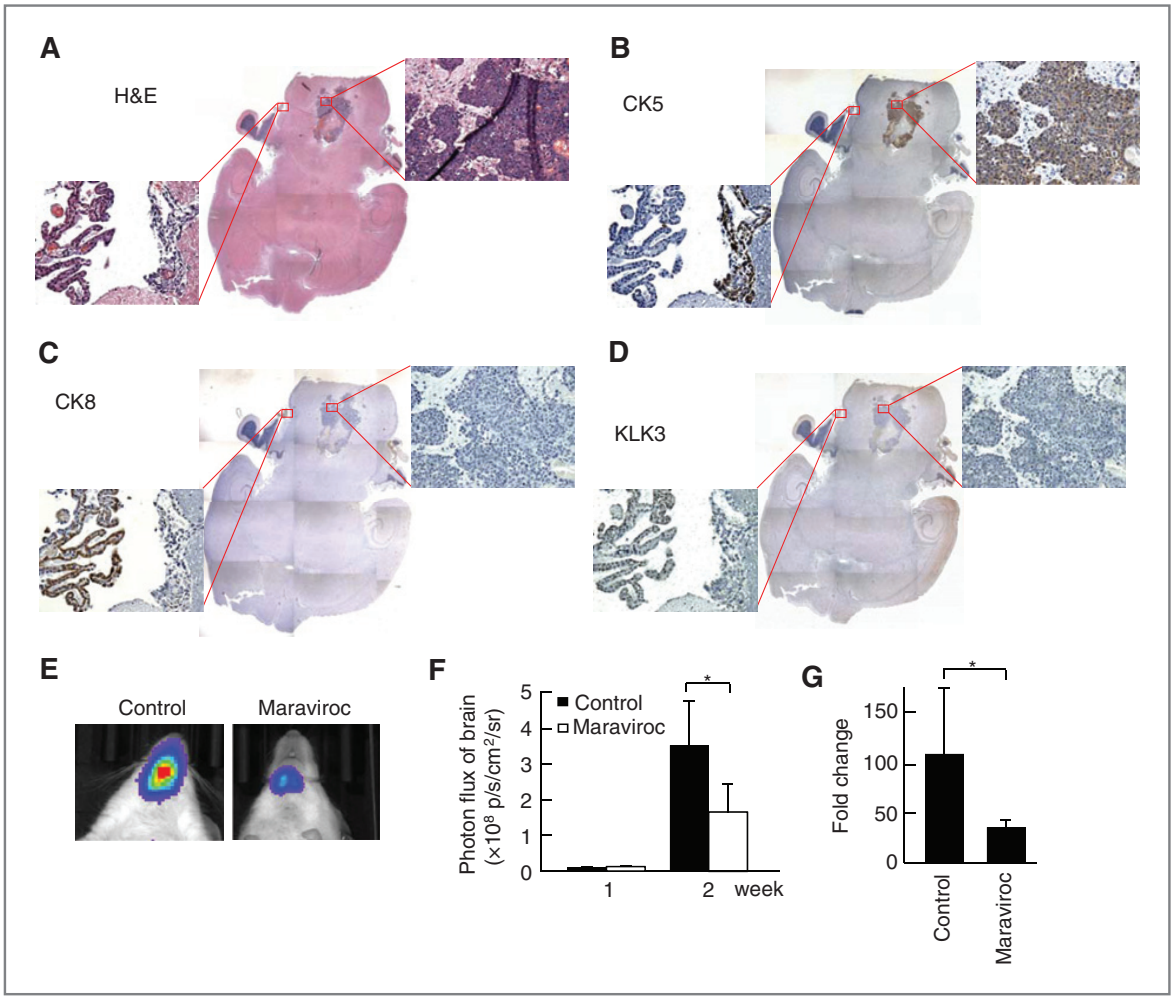

Figure 7. Maraviroc treatment reduces v-Src-PEC brain metastasis. A–D, histologic images of v-Src-PEC brain metastasis in FVB mice showing H&E staining (A) or immunohistochemical staining for CK5 (B), CK8 (C), or KLK3 (D). E, representative images of photonic flux from brain metastasis of FVB mice v-Src-PEC tumor treated with a CCR5 inhibitor maraviroc or control with quantitation of mean photon flux (F) or mean fold change in photon flux 1 versus 2 weeks (G). The 70-fold reduction in photon emission from brain metastasis in the maraviroc-treated group is significant ($P < 0.001$). The data are mean ±SEM for $N > 5$ separate experiments.

(Supplementary Fig. SS7D–S7G). This finding raises the possibility that activation of CCR5 signaling can contribute to the poor outcome in this subset of patients.

What might be the clinical implications of the current preclinical studies? The prognosis for men with metastatic prostate cancer is on average 30 to 35 months. Radiation treatment for local sites and radiopharmaceuticals, such as strontium-89, samarium-153, and rhenium-188-HEDP, has demonstrated improvements in palliation. Herein oral administration of the CCR5 inhibitor maraviroc, an FDA-approved compound used for treatment of HIV deployed at similar dose as that used in the clinic, reduced the metastatic burden by approximately 80% and metastatic bone burden by >60%. Given the relative enrichment of CCR5 signaling in patients with poor prognosis prostate cancer and the preclinical efficacy of CCR5 inhibitors herein, the current studies of CCR5 inhibitors suggest clinical trials may be warranted in human prostate cancer patients, with tumors enriched for this pathway.

Disclosure of Potential Conflicts of Interest

R.G.Pestell holds ownership interests in and serves as CSO/Founder of the biopharmaceutical companies ProstaGene, LLC and AAA Phoenix, Inc. R.G. Pestell additionally holds ownership interests (value unknown) for several submitted patent applications. No potential conflicts of interest were disclosed by the other authors.

Authors' Contributions

Conception and design: X. Jiao, M. Velasco-Velazquez, M.P. Lisanti, R.G. Pestell
Development of methodology: D. Sicoli, X. Jiao, X. Ju, Z. Li, A. Fatatis, B. Paudyal, M.L. Thakur, R.G. Pestell
Acquisition of data (provided animals, acquired and managed patients, provided facilities, etc.): D. Sicoli, X. Jiao, X. Ju, M. Velasco-Velazquez, B. Paudyal, M.L. Thakur, R.G. Pestell

Analysis and interpretation of data (e.g., statistical analysis, biostatistics, computational analysis): D. Sicoli, X. Jiao, X. Ju, A. Ertel, S. Addya, A. Fatatis, B. Paudyal, M.L. Thakur, R.G. Pestell
Writing, review, and/or revision of the manuscript: D. Sicoli, X. Jiao, X. Ju, M. Velasco-Velazquez, A. Fatatis, B. Paudyal, M. Cristofanilli, M.L. Thakur, M.P. Lisanti, R.G. Pestell
Administrative, technical, or material support (i.e., reporting or organizing data, constructing databases): X. Jiao, X. Ju, R.G. Pestell
Study supervision: X. Jiao, X. Ju, S. Andò, R.G. Pestell

Grant Support

This work was supported in part by NIH grants R01CA070896, R01CA075503, R01CA132115, R01CA107382, R01CA086072 (R.G. Pestell), R01CA120876 (M.P. Lisanti), the Kimmel Cancer Center NIH Cancer Center Core grant P30CA056036 (R.G. Pestell), generous grants from the Dr. Ralph and Marian C. Falk Medical Research Trust (R.G. Pestell), the Margaret Q. Landenberger Research Foundation (M.P. Lisanti), a grant from Pennsylvania Department of Health (R.G. Pestell) and PAPIIT-UNAM IN219613 (M.A. Velasco-Velazquez). M.P. Lisanti and his laboratory were supported via the resources of Thomas Jefferson University (Philadelphia, PA).

The costs of publication of this article were defrayed in part by the payment of page charges. This article must therefore be hereby marked *advertisement* in accordance with 18 U.S.C. Section 1734 solely to indicate this fact.

Received March 4, 2014; revised August 21, 2014; accepted September 3, 2014; published online December 1, 2014.

References

1. Jemal A, Murray T, Samuels A, Ghafoor A, Ward E, Thun MJ. Cancer statistics, 2003. CA Cancer J Clin 2003;53:5–26.
2. Tatarov O, Mitchell TJ, Seywright M, Leung HY, Brunton VG, Edwards J. SRC family kinase activity is up-regulated in hormone-refractory prostate cancer. Clin Cancer Res 2009;15:3540–9.
3. Fizazi K. The role of Src in prostate cancer. Ann Oncol 2007;18:1765–73.
4. Cai H, Smith DA, Memarzadeh S, Lowell CA, Cooper JA, Witte ON. Differential transformation capacity of Src family kinases during the initiation of prostate cancer. Proc Natl Acad Sci U S A 2011;108:6579–84.
5. Scher HI, Sawyers CL. Biology of progressive, castration-resistant prostate cancer: directed therapies targeting the androgen-receptor signaling axis. J Clin Oncol 2005;23:8253–61.
6. Cai H, Babic I, Wei X, Huang J, Witte ON. Invasive prostate carcinoma driven by c-Src and androgen receptor synergy. Cancer Res 2011;71:862–72.
7. Kraus S, Gioeli D, Vomastek T, Gordon V, Weber MJ. Receptor for activated C kinase 1 (RACK1) and Src regulate the tyrosine phosphorylation and function of the androgen receptor. Cancer Res 2006;66:11047–54.
8. Migliaccio A, Castoria G, Di Domenico M, de Falco A, Bilancio A, Lombardi M, et al. Steroid-induced androgen receptor-oestradiol receptor beta-Src complex triggers prostate cancer cell proliferation. EMBO J 2000;19:5406–17.
9. Mundy GR. Metastasis to bone: causes, consequences and therapeutic opportunities. Nat Rev Cancer 2002;2:584–93.
10. Noguchi M, Kikuchi H, Ishibashi M, Noda S. Percentage of the positive area of bone metastasis is an independent predictor of disease death in advanced prostate cancer. Br J Cancer 2003;88:195–201.
11. Roodman GD. Mechanisms of bone metastasis. N Engl J Med 2004;350:1655–64.
12. Fidler IJ. Understanding bone metastases: the key to the effective treatment of prostate cancer. Clin Adv Hematol Oncol 2003;1:278–9.
13. Kim SJ, Uehara H, Yazici S, He J, Langley RR, Mathew P, et al. Modulation of bone microenvironment with zoledronate enhances the therapeutic effects of STI571 and paclitaxel against experimental bone metastasis of human prostate cancer. Cancer Res 2005;65:3707–15.
14. Shen MM, Abate-Shen C. Molecular genetics of prostate cancer: new prospects for old challenges. Genes Dev 2010;24:1967–2000.
15. Irshad S, Abate-Shen C. Modeling prostate cancer in mice: something old, something new, something premalignant, something metastatic. Cancer Metastasis Rev 2013;32:109–22.
16. Ju X, Ertel A, Casimiro MC, Yu Z, Meng H, McCue PA, et al. Novel oncogene-induced metastatic prostate cancer cell lines define human prostate cancer progression signatures. Cancer Res 2013;73:978–89.
17. Liu H, Patel MR, Prescher JA, Patsialou A, Qian D, Lin J, et al. Cancer stem cells from human breast tumors are involved in spontaneous metastases in orthotopic mouse models. Proc Natl Acad Sci U S A 2010;107:18115–20.
18. Desai B, Rogers MJ, Chellaiah MA. Mechanisms of osteopontin and CD44 as metastatic principles in prostate cancer cells. Mol Cancer 2007;6:18.
19. Bondareva A, Downey CM, Ayres F, Liu W, Boyd SK, Hallgrimsson B, et al. The lysyl oxidase inhibitor, beta-aminopropionitrile, diminishes the metastatic colonization potential of circulating breast cancer cells. PLoS ONE 2009;4:e5620.
20. Jiao X, Katiyar S, Willmarth NE, Liu M, Ma X, Flomenberg N, et al. c-Jun induces mammary epithelial cellular invasion and breast cancer stem cell expansion. J Biol Chem 2010;285:8218–26.
21. Russell MR, Liu Q, Fatatis A. Targeting the {alpha} receptor for platelet-derived growth factor as a primary or combination therapy in a preclinical model of prostate cancer skeletal metastasis. Clin Cancer Res 2010;16:5002–10.
22. Power CA, Pwint H, Chan J, Cho J, Yu Y, Walsh W, et al. A novel model of bone-metastatic prostate cancer in immunocompetent mice. Prostate 2009;69:1613–23.
23. Thudi NK, Martin CK, Nadella MV, Fernandez SA, Werbeck JL, Pinzone JJ, et al. Zoledronic acid decreased osteolysis but not bone metastasis in a nude mouse model of canine prostate cancer with mixed bone lesions. Prostate 2008;68:1116–25.
24. Ralis ZA, Watkins G. Modified tetrachrome method for osteoid and defectively mineralized bone in paraffin sections. Biotech Histochem 1992;67:339–45.
25. Schalken JA, van Leenders G. Cellular and molecular biology of the prostate: stem cell biology. Urology 2003;62:11–20.
26. Velasco-Velazquez M, Jiao X, De La Fuente M, Pestell TG, Ertel A, Lisanti MP, et al. CCR5 antagonist blocks metastasis of basal breast cancer cells. Cancer Res 2012;72:3839–50.
27. Trotman LC, Niki M, Dotan ZA, Koutcher JA, Di Cristofano A, Xiao A, et al. Pten dose dictates cancer progression in the prostate. PLoS Biol 2003;1:E59.
28. Ding Z, Wu CJ, Chu GC, Xiao Y, Ho D, Zhang J, et al. SMAD4-dependent barrier constrains prostate cancer growth and metastatic progression. Nature 2011;470:269–73.
29. Wang J, Kobayashi T, Floc'h N, Kinkade CW, Aytes A, Dankort D, et al. B-Raf activation cooperates with PTEN loss to drive c-Myc expression in advanced prostate cancer. Cancer Res 2012;72:4765–76.
30. Sethi N, Kang Y. Unravelling the complexity of metastasis - molecular understanding and targeted therapies. Nat Rev Cancer 2011;11:735–48.
31. Kang Y, Siegel PM, Shu W, Drobnjak M, Kakonen SM, Cordon-Cardo C, et al. A multigenic program mediating breast cancer metastasis to bone. Cancer Cell 2003;3:537–49.
32. Bos PD, Zhang XH, Nadal C, Shu W, Gomis RR, Nguyen DX, et al. Genes that mediate breast cancer metastasis to the brain. Nature 2009;459:1005–9.
33. Minn AJ, Gupta GP, Siegel PM, Bos PD, Shu W, Giri DD, et al. Genes that mediate breast cancer metastasis to lung. Nature 2005;436:518–24.
34. Clark EA, Golub TR, Lander ES, Hynes RO. Genomic analysis of metastasis reveals an essential role for RhoC. Nature 2000;406:532–5.
35. Yang J, Mani SA, Donaher JL, Ramaswamy S, Itzykson RA, Come C, et al. Twist, a master regulator of morphogenesis, plays an essential role in tumor metastasis. Cell 2004;117:927–39.

36. Gumireddy K, Sun F, Klein-Szanto AJ, Gibbins JM, Gimotty PA, Saunders AJ, et al. In vivo selection for metastasis promoting genes in the mouse. Proc Natl Acad Sci U S A 2007;104:6696–701.
37. Lee F, Jure-Kunkel MN, Salvati ME. Synergistic activity of ixabepilone plus other anticancer agents: preclinical and clinical evidence. Ther Adv Med Oncol 2011;3:11–25.
38. Orphanos GS, Ioannidis GN, Ardavanis AG. Cardiotoxicity induced by tyrosine kinase inhibitors. Acta Oncol 2009;48:964–70.
39. Dalton RN, Chetty R, Stuart M, Iacona RB, Swaisland A. Effects of the Src inhibitor saracatinib (AZD0530) on renal function in healthy subjects. Anticancer Res 2010;30:2935–42.
40. Giehl M, Leitner A, Haferlach C, Duesberg P, Hofmann WK, Hofheinz R, et al. Detection of centrosome aberrations in disease-unrelated cells from patients with tumor treated with tyrosine kinase inhibitors. Eur J Haematol 2010;85:139–48.
41. Aleshin A, Finn RS. SRC: a century of science brought to the clinic. Neoplasia 2010;12:599–607.

CCR5 Receptor Antagonists Block Metastasis to Bone of v-Src Oncogene–Transformed Metastatic Prostate Cancer Cell Lines

Daniela Sicoli, Xuanmao Jiao, Xiaoming Ju, et al.

Cancer Res 2014;74:7103-7114.